Interaction and entanglement engineering in a driven-giant-atom setup with a coupled resonator waveguide

Mingzhu Weng,[1] Xin Wang,[2] and Zhihai Wang[1,*]

[1]*Center for Quantum Sciences and School of Physics, Northeast Normal University, Changchun 130024, China*

[2]*Institute of Theoretical Physics, School of Physics, Xi'an Jiaotong University, Xi'an 710049, People's Republic of China*

(Received 26 January 2024; revised 27 July 2024; accepted 1 August 2024; published 19 August 2024)

We investigate the coherent interactions mediated by the coupled resonator waveguide between two types of giant atoms. We find that the effective coupling and collective dissipation can be controlled on demand by adjusting the configuration of the giant atoms. As a result, the external driving gives birth to a substantial steady-state entanglement between two giant atoms, which exhibits a Rabi splitting character. In the three-giant-atom setup, we find that the nonzero next neighbor atomic entanglement can surpass the neighbor ones and is able to be adjusted by tuning the driving phase, which serves as an artificial magnetic field. The enhancement of next neighbor atomic entanglement cannot be realized in the small-atom setup. We hope these controllable interactions in giant-atom arrays are useful applications in the quantum information process.

DOI: 10.1103/PhysRevA.110.023721

I. INTRODUCTION

The light-matter interaction plays a crucial role in fundamental science, supporting the rapid development of quantum technology [1,2]. In the conventional treatment for the light-matter interactions, the atoms are usually viewed as the point-shaped dipoles [3]. However, the realization of coupling between the superconducting transmon and the surface acoustic wave (SAW) has promoted the size of the matter (i.e., the transmon) to be comparable to the wavelength of the SAW [4] and the dipole approximation is broken [4–10]. Such a paradigm is subsequently named "giant atom," to differ from the traditional "small atom." The nonlocal coupling between the giant atom and the waveguide promises to observe a lot of fascinating phenomena, such as frequency-dependent atomic relaxation rates and Lamb shifts [11–13], nonexponential atomic decay [14–16], exotic atom-photon bound states [17–21], non-Markovian decay dynamics [22–26], and chiral light-matter interactions [27–31]. Experimentally, the giant-atom structures have also been realized in superconducting quantum circuits [32,33], coupled waveguide arrays [34], and ferromagnetic spin systems [35]. Besides, there are some theoretical proposals in cold atoms within the optical lattices [36] as well as the synthetic frequency dimensions [37,38].

As for the multiple giant atoms, the waveguide can serve as a data bus, to induce the coherent interaction [39], where the geometrical configuration of the giant atom serves as a sensitive controller. For the two-giant-atom setup, the braided coupling [27,33,40], nested coupling [41,42] has been predicted to be useful in some quantum information processing by constructing the decoherence-free interaction [42–44] and generating robust entanglement [11,45–49].

In the viewpoint of the open quantum system, the wide energy band structure of the coupled resonator waveguide supplies an environment for the giant atom, to introduce the possible individual and collective atomic dissipation. One of the actionable concerned topics is the nonequilibrium dynamics of the open system which is subject to the external driven and dissipation [50–55]. In this community, great efforts have been made to realize steady-state entanglement between quantum emitters for various quantum information processing. For example, the remote multiple entanglement scheme in two separated channels which are simultaneously driven by parametric down-conversion processes is proposed for the quantum network [56,57]. Moreover, the remote entanglement has also been investigated in the giant-atom setup, where the nonlocal coupling takes great roles [47,49,58,59]. In the above works, the "remote" usually refers to the fact that the entangled emitters are distant from each other, but leave the inside space empty. However, a more realistic need in the quantum network is to realize the entanglement between target nodes which are separated by other nodes, that is, the non-nearest quantum nodes.

In this paper, we tackle the above issues by considering an array of giant atoms which couple to the coupled resonator waveguide. After tracing out the degree of freedom of the waveguide, we reach three cases of effective interaction and collective dissipation among the giant atoms. By controlling the strength and the phase of the driving fields, we find that the steady-state entanglement can be engineered on demand. More interestingly, we find that there is the cyclic energy diagram in the three-giant-atom setup. This allows the phase of the external driving which serves as the artificial gauge field [60–66] to enhance the next neighbor atomic entanglement so as to surpass the neighbor atomic entanglement. It is not possible in the small-atom counterpart.

The rest of the paper is organized as follows. In Sec. II, we describe our model and discuss the controllable effective

*Contact author: wangzh761@nenu.edu.cn

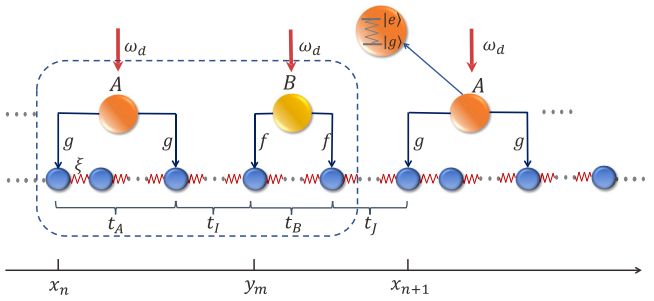

FIG. 1. Sketch of giant atoms coupled to a 1D coupled-resonator waveguide, where two types of giant atoms are arranged alternately. The odd (even) number of giant atoms are labeled as A (B) represented by an orange ball (yellow ball).

coupling and collective dissipation induced by the waveguide. In Sec. III, we discuss the dynamic behavior and the steady-state entanglement of the system in the two-giant-atom configuration. In Sec. IV, we generalize to the three-giant-atom setup and the steady-state entanglement behavior of the system was discussed in comparison with the small-atom configuration. In Sec. V, we discuss the manipulation of the steady state entanglement by tuning the driving phase. In Sec. VI, we provide a short summary and discussion. Some detailed derivations of the master equation for giant atoms and small atoms are given in the Appendixes.

II. MODEL AND MASTER EQUATION

We consider an array of two-level giant atoms which interacts with a one-dimensional coupled-resonator waveguide as sketched in Fig. 1. The giant atomic array is composed of two types of giant atoms (labeled A and B in Fig. 1) which are arranged alternately with numbers being N and M, respectively, and each giant atom couples to the waveguide at two sites. The Hamiltonian of the system is written as $H = H_c + H_a + H_I$ ($\hbar = 1$),

$$H_c = \omega_c \sum_j a_j^\dagger a_j - \xi \sum_j (a_{j+1}^\dagger a_j + a_j^\dagger a_{j+1}), \tag{1}$$

$$H_a = \frac{\Omega}{2}\sum_n \sigma_z^{(n)} + \frac{\Omega}{2}\sum_m \Gamma_z^{(m)}, \tag{2}$$

$$H_I = g\sum_n \left[\left(a_{x_n}^\dagger + a_{x_n+t_A}^\dagger\right)\sigma_-^{(n)} + \text{H.c.}\right] + f\sum_m \left[\left(a_{y_m}^\dagger + a_{y_m+t_B}^\dagger\right)\Gamma_-^{(m)} + \text{H.c.}\right]. \tag{3}$$

Here ω_c is the frequency of the resonators, a_j is the annihilation operator on site j, and ξ refers to the neighbor coupling strength. The spacing between all neighboring resonators in the coupled-resonator waveguide is set as the unit of length. $\sigma_\pm(\Gamma_\pm)$ are the Pauli operators of the giant atom $A(B)$; Ω is the transition frequency of the giant atom between the ground state $|g\rangle$ and the excited state $|e\rangle$. Note that g, f are the coupling strengths of A and B giant atoms with the waveguide, respectively. $t_A(t_B)$ characterizes the size of the giant atom $A(B)$. Giant atom A in the nth cell is coupled to the waveguide at site x_n and $x_n + t_A$, $n = 1, 2, \ldots, N$. Similarly, the coupling site of the B giant atom within the same cell is y_m and $y_m + t_B$, $m = 1, 2, \ldots, M$. $y_i = x_i + t_A + t_I$ and $x_i = y_{i-1} + t_B + t_J$ with the parameter t_I, t_J being the intracell atomic distance and the extra-cell atomic distance, respectively.

Considering the length of the waveguide $N_c \to \infty$, we can rewrite the Hamiltonian of the system in momentum space. By introducing the Fourier transformation $a_j = \sum_k a_k e^{ikj}/\sqrt{N_c}$, the Hamiltonian H_c becomes $H_k = \sum_k \omega_k a_k^\dagger a_k$ with the dispersion relation being given by $\omega_k = \omega_c - 2\xi\cos k$. Therefore, the waveguide supports a single-photon continual band with center frequency ω_c and a bandwidth 4ξ. In the momentum space, the atom-waveguide coupling Hamiltonian H_I is expressed as

$$H_I = \frac{g}{\sqrt{N_c}}\sum_{n,k}[a_k^\dagger(e^{-ikx_n} + e^{-ik(x_n+t_A)})\sigma_-^{(n)} + \text{H.c.}] + \frac{f}{\sqrt{N_c}}\sum_{m,k}[a_k^\dagger(e^{-iky_m} + e^{-ik(y_m+t_B)})\Gamma_-^{(m)} + \text{H.c.}]. \tag{4}$$

Let us first consider the weak-coupling or broadband limit $g, f \ll \xi$. In this regime, the waveguide modes can be eliminated by adopting the Born-Markov approximation. To obtain the master equation for the density matrix of the giant atoms, we work in the momentum representation and the interaction picture. Then, the interaction Hamiltonian H_I becomes [67]

$$H_I = g\sum_n [\sigma_+^{(n)}E(x_n,t)e^{i\Omega t} + \sigma_+^{(n)}E(x_n+t_A,t)e^{i\Omega t} + \text{H.c.}] + f\sum_m [\Gamma_+^{(m)}E(y_m,t)e^{i\Omega t} + \Gamma_+^{(m)}E(y_m+t_B,t)e^{i\Omega t} + \text{H.c.}], \tag{5}$$

where $E(X,t) = \frac{1}{\sqrt{N_c}}\sum_k e^{-i\omega_k t}e^{ikX}a_k$ is the field operator at site X and the master equation is formally written as [68]

$$\frac{d}{dt}\rho(t) = -\int_0^\infty d\tau\, \text{Tr}_c\{[H_I(t),[H_I(t-\tau),\rho_c\otimes\rho(t)]]\}. \tag{6}$$

In what follows, we will consider that the giant atoms are resonant with the bare resonator, that is, $\Omega = \omega_c$. As a result, we obtain a master equation for the reduced density operator of the giant atoms (the detailed calculations are given in Appendix A) as

$$\begin{aligned}\dot{\rho} = &-i[\mathcal{H},\rho] \\ &+\sum_{n,m}[g^2U_{11}^{(n,m)}(2\sigma_-^{(n)}\rho\sigma_+^{(m)} - \sigma_+^{(m)}\sigma_-^{(n)}\rho - \rho\sigma_+^{(n)}\sigma_-^{(m)}) \\ &+f^2U_{22}^{(n,m)}(2\Gamma_-^{(n)}\rho\Gamma_+^{(m)} - \Gamma_+^{(n)}\Gamma_-^{(m)}\rho - \rho\Gamma_+^{(n)}\Gamma_-^{(m)}) \\ &+gfU_{12}^{(n,m)}(2\sigma_-^{(n)}\rho\Gamma_+^{(m)} - \sigma_+^{(n)}\Gamma_-^{(m)}\rho - \rho\sigma_+^{(n)}\Gamma_-^{(m)}) \\ &+gfU_{21}^{(n,m)}(2\Gamma_-^{(n)}\rho\sigma_+^{(m)} - \Gamma_+^{(n)}\sigma_-^{(m)}\rho - \rho\Gamma_+^{(n)}\sigma_-^{(m)})],\end{aligned} \tag{7}$$

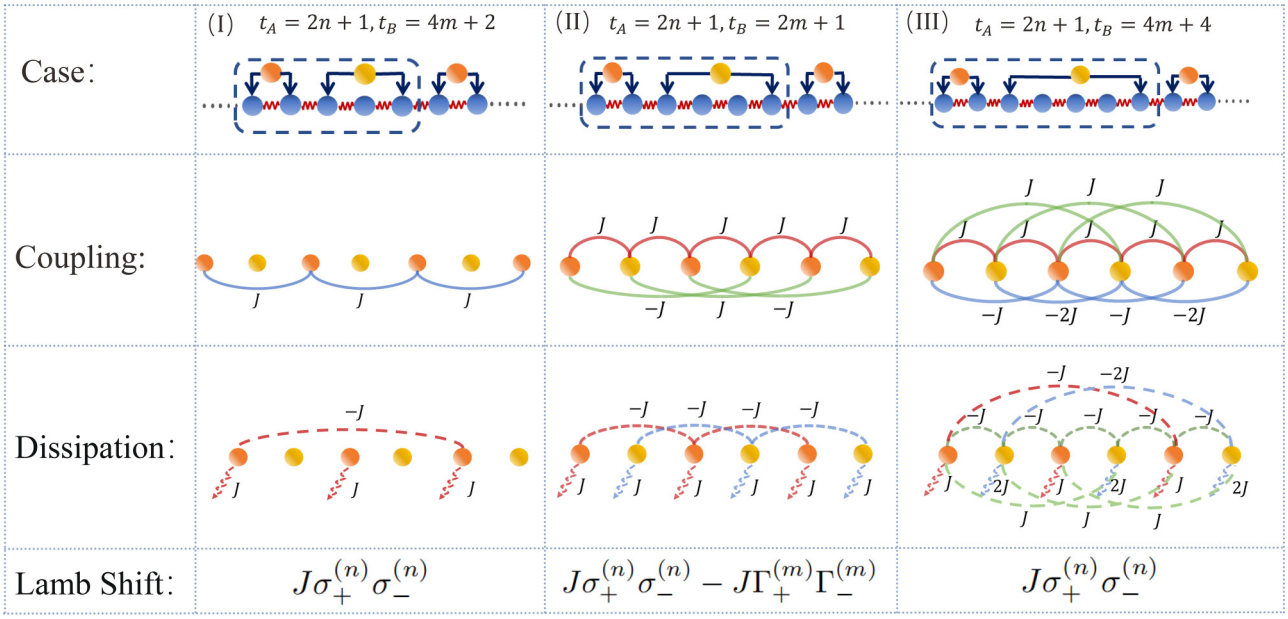

FIG. 2. Effective couplings and dissipations for three different cases. The first line is the schematic illustration of different systems of the odd (even) number of atoms labeled as A (B) and represented by an orange (yellow) ball. The second line corresponds to a schematic diagram of the corresponding effective coherent interaction, that is, the neighbor interaction (red solid line), the next neighbor interaction (blue solid line), and the secondary neighbor interaction (green solid line). The third line shows the diagram of collective dissipation, in which the dissipation between A atoms is represented by the red dashed line, the dissipation between B atoms is represented by the blue dashed line, and the collective dissipation between $A-B$ atoms is represented by the green dashed line. The red wave line is the independent dissipation induced by the waveguide. The last line is the Lamb shift induced by the waveguide. $J = g^2/\xi$ with $g = f$ being the coupling strength between the giant atoms and the waveguide.

where the coherent coupling between the atoms is described by the Hamiltonian

$$\begin{aligned}\mathcal{H} = &\sum_{n,m}\left(\frac{\Omega}{2}\sigma_z^{(n)} + \frac{\Omega}{2}\Gamma_z^{(m)}\right)\\ &+\sum_{n,m}[g^2 I_{11}\sigma_+^{(n)}\sigma_-^{(m)} + f^2 I_{22}\Gamma_+^{(n)}\Gamma_-^{(m)}]\\ &+\sum_{n,m}[gf(I_{12}\sigma_+^{(n)}\Gamma_-^{(m)} + I_{21}\Gamma_+^{(n)}\sigma_-^{(m)})].\end{aligned} \tag{8}$$

In the above equations, we have defined $U_{ij} = \mathrm{Re}(A_{ij})$, $I_{ij} = \mathrm{Im}(A_{ij})(i, j = 1, 2)$ with

$$A_{11} = \sum_n\sum_m \frac{1}{2\xi}(2e^{i\frac{\pi}{2}|x_n - x_m|} + e^{i\frac{\pi}{2}|x_n - x_m - t_A|} + e^{i\frac{\pi}{2}|x_n + t_A - x_m|}), \tag{9}$$

$$A_{22} = \sum_n\sum_m \frac{1}{2\xi}(2e^{i\frac{\pi}{2}|y_n - y_m|} + e^{i\frac{\pi}{2}|y_n - y_m - t_B|} + e^{i\frac{\pi}{2}|y_n + t_B - y_m|}), \tag{10}$$

$$\begin{aligned}A_{12} = &\sum_n\sum_m \frac{1}{2\xi}(e^{i\frac{\pi}{2}|x_n - y_m|} + e^{i\frac{\pi}{2}|x_n - y_m - t_B|}\\ &+ e^{i\frac{\pi}{2}|x_n + t_A - y_m|} + e^{i\frac{\pi}{2}|x_n + t_A - y_m - t_B|}),\end{aligned} \tag{11}$$

$$\begin{aligned}A_{21} = &\sum_n\sum_m \frac{1}{2\xi}(e^{i\frac{\pi}{2}|y_n - x_m|} + e^{i\frac{\pi}{2}|y_n - y_m - t_A|}\\ &+ e^{i\frac{\pi}{2}|y_n + t_B - x_m|} + e^{i\frac{\pi}{2}|y_n + t_B - x_m - t_A|}).\end{aligned} \tag{12}$$

From the above formula, it can be seen that the coherent interaction and the collective dissipation between the giant atoms can be modulated by the size of each giant atom, that is, the distance between the atom-waveguide coupling points. For simplicity, we consider that the two kinds of giant atoms couple to the waveguide via the same coupling strength at each site and fix the atomic spacing to be uniform by setting $f = g$, $t_I = t_J = 1$.

By adjusting the size of the giant atoms on demand, we can obtain the following three cases of effective coherent couplings and collective dissipations, which are listed in Fig. 2. Now, we illustrate them in detail. Case (I): when $t_A = 2n+1$, $t_B = 4m+2$ with integral $n, m = 0, 1, 2\ldots$, we find that $A_{22} = 0$, $A_{12} = 0$, and $A_{21} = 0$. Therefore, the B giant atoms are totally decoupled from the waveguide due to the interference effect between the two connecting points. As for the A type giant atoms, they undergo the coherent coupling, with both individual and collective dissipations. Case (II): when $t_A = 2n+1$, $t_B = 2m+1$, the effective coherent couplings only exist between the different types of the atoms. Meanwhile, the collective dissipation occurs between the same types of the atoms except for their individual dissipations. Case (III): when $t_A = 2n+1$, $t_B = 4m+4$, both

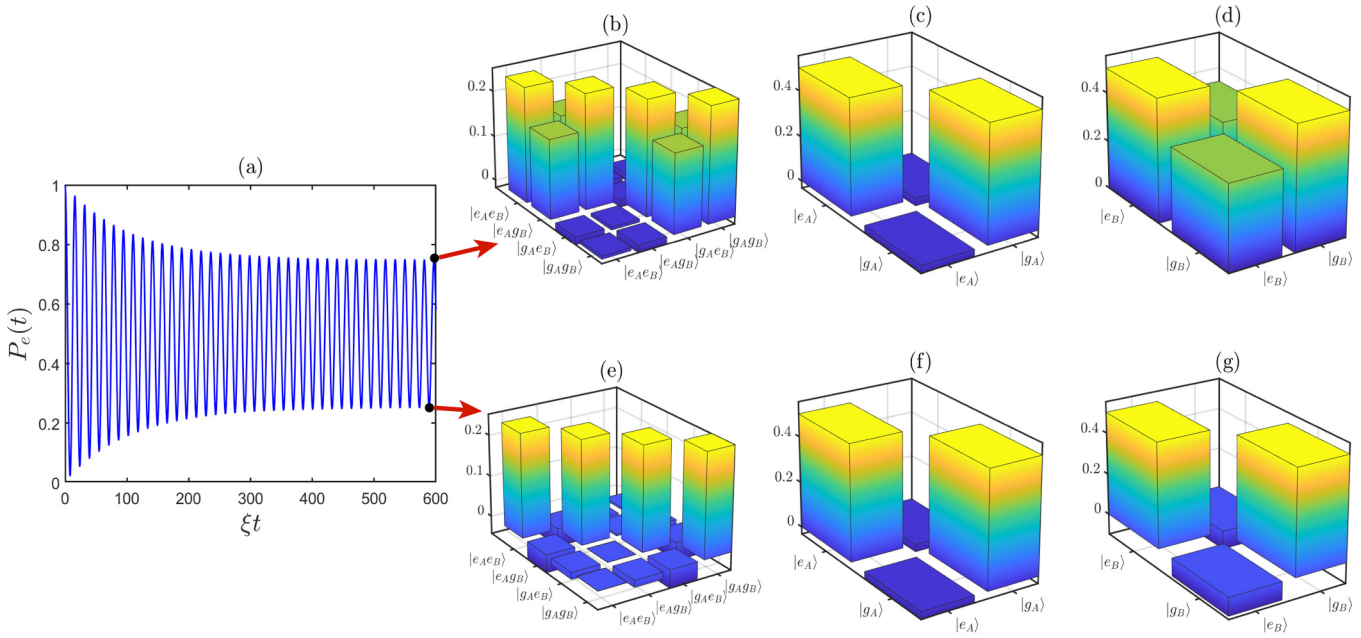

FIG. 3. (a) Time evolution of the average value of the Pauli operators $P_e(t) = (\langle\sigma_z\rangle + \langle\Gamma_z\rangle)/2$. (b)–(g) Tomography of the state of the system at different moments. The parameters are set as $\Delta = 0$, $g = f = 0.08\xi$, and $\eta = 0.2\xi$.

of the two types of the giant atoms undergo the individual dissipations. Moreover, the coupling and collective dissipations exist between both of the same and different types of giant atoms. Besides the mentioned statements above, one of the most intriguing differences between the coherent couplings is that, in case (III), only three atoms are needed to form the cyclic coupling, whereas in case (II) at least four are needed.

Note that there are still three other configurations which are not illustrated in Fig. 2. They are $t_A = 4n + 2$, $t_B = 4m + 4$, $t_A = 4n + 2$, $t_B = 4m + 2$ and $t_A = 4n + 4$, $t_B = 4m + 4$, respectively. For $t_A = 4n + 2$, $t_B = 4m + 4$ and $t_A = 4n + 2$, $t_B = 4m + 2$, both of the two types of the giant atoms are totally decoupled from the waveguide with $A_{11} = A_{22} = A_{12} = A_{21} = 0$. When $t_A = 4n + 4$, $t_B = 4m + 4$, it has the same form of the coherence coupling form as case (II) in Fig. 2. Therefore, we will not discuss them in what follows. Based on the three cases listed in Fig. 2, we will discuss the dynamical behavior for the two- and three-giant-atoms setup. The results for the small-atom setup will be listed in Appendix B for comparison.

III. TWO GIANT ATOMS

In this section, we first discuss only the two-giant-atoms setup, which are labeled by A and B, respectively. A general master equation can be written as

$$\dot{\rho} = -i[\mathcal{H} + H_d, \rho] + J_1 D_{[\sigma_+,\sigma_-]\rho} + J_2 D_{[\Gamma_+,\Gamma_-]\rho} + J_3(D_{[\sigma_+,\Gamma_-]\rho} + D_{[\Gamma_+,\sigma_-]\rho}), \tag{13}$$

where $\mathcal{H}$ is the effective Hamiltonian and $D_{[O_1,O_2]\rho} = 2O_2\rho O_1 - \rho O_1 O_2 - O_1 O_2 \rho$. The Hamiltonian $\mathcal{H}$ and the coefficients J_i $(i = 1, 2, 3)$ depend on the configuration of the giant atoms. In the rotating frame, the driving Hamiltonian is written as $H_d = \eta(\sigma_+ + \Gamma_+ + \text{H.c.})$. Here, the driving field is applied directly to the atoms and does not cause the interactions between the atoms. We will use the notation $\mathcal{H}_{\rm I}(\mathcal{H}_{\rm II}, \mathcal{H}_{\rm III})$ to represent the effective Hamiltonian for case (I) [case (II) and case (III)].

For the (I) case of $t_A = 2n + 1$, $t_B = 4m + 2$ with integral $n, m = 0, 1, 2\ldots$, the Hamiltonian is

$$\mathcal{H}_{\rm I} = \Delta\sigma_z + \Delta\Gamma_z + J\sigma_+\sigma_-, \tag{14}$$

where $J = g^2/\xi$ and $\Delta = \Omega - \omega_d$ is the detuning between the frequency of the giant atoms and the frequency of driving field. The coefficients in the dissipation terms satisfy $J_1 = J$ and $J_i = 0$ for $i = 2, 3$. We now consider that the two giant atoms are both excited initially ($|\psi(0)\rangle = |e, e\rangle$) and explore the time evolution of the atomic populations. In Fig. 3(a), we find that the system cannot reach a steady state even when the evolution time tends to be infinity. The distinguished dynamics for the giant atoms can be explained by the cartoon coupling scheme in the first column of Fig. 2. The two giant atoms are isolated from each other with neither effective coupling nor collective decay. The giant atom A experiences both the dissipation induced by the waveguide and the external driving field and eventually achieves its steady state. On the contrary, the giant atom B is subject only to the external driving field and exhibits the Rabi oscillation. We further pick two points $\xi t = 597$ and $\xi t = 589$ among the moments during the time evolution when the atomic population achieves its maximum and minimum values in Fig. 3(a) and tomograph the corresponding quantum state in Figs. 3(b) and 3(e). It shows that the population exhibits a uniform distribution diagonally for both of the two states. However, unlike the obvious coherence in the bare basis of the two atom $\rho_{e_Ag_B,e_Ae_B} = 0.1712$ as shown in Fig. 3(b), the coherence of the steady state is $\rho_{e_Ag_B,e_Ae_B} = 0.04$ shown in Fig. 3(e). The

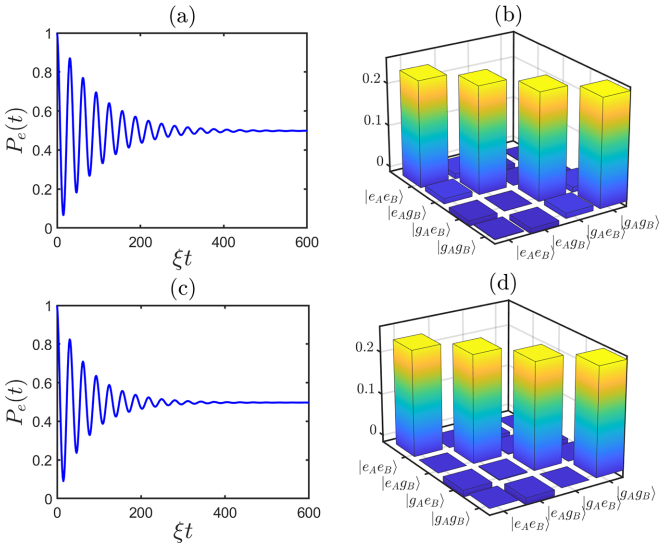

FIG. 4. Giant atomic population evolution (a), (c) and the tomography of the steady state (b), (d). The results for cases (II) and (III) are demonstrated in (a), (b) and (c), (d), respectively. The parameters are set as $\Delta = 0$, $g = f = 0.08\xi$, and $\eta = 0.2\xi$.

latter one is only 0.2 times the former one, so the coherence shown in Fig. 3(e) can be neglected. In Figs. 3(c), 3(d), 3(f), and 3(g), we further illustrate the tomography of the reduced density matrix $\rho_{A(B)} = \mathrm{Tr}_{B(A)}\rho$ in the two states in order to investigate the states of the atoms A and B, respectively. At these two moments, the states of the giant atom A are the same as shown in Figs. 3(c) and 3(f), but the giant atom B behaves differently as shown in Figs. 3(d) and 3(g). Therefore, the unstable behavior originates from the isolated giant atom B, which is continuously driven by the external driving field.

As shown in Fig. 2, the effective Hamiltonians for the (II) and (III) cases become

$$\mathcal{H}_{\mathrm{II}} = \Delta\sigma_z + \Delta\Gamma_z + J\sigma_+\sigma_- - J\Gamma_+\Gamma_- + J(\sigma_+\Gamma_- + \Gamma_+\sigma_-), \tag{15}$$

$$\mathcal{H}_{\mathrm{III}} = \Delta\sigma_z + \Delta\Gamma_z + J\sigma_+\sigma_- + J(\sigma_+\Gamma_- + \Gamma_+\sigma_-). \tag{16}$$

The effective coupling is identical in both cases, while the only differences come from the Lamb shift term induced by the waveguide. As for the dissipation counterpart, we have $J_1 = J_2 = J, J_3 = 0$ for case (II) and $J_1 = J$, $J_2 = 2J$, $J_3 = -J$ for case (III), respectively. Due to the similarity between the above two effective Hamiltonians $\mathcal{H}_{\mathrm{II}}$ and $\mathcal{H}_{\mathrm{III}}$, we observe that the system will undergo an initial oscillation and finally reach the steady state in the (II) and (III) cases, whose dynamics are demonstrated in Figs. 4(a) and 4(c), respectively. For the steady state, the tomography results in Figs. 4(b) and 4(d) show that they are almost the maximum mixed state without obvious coherence terms.

We furthermore explore the steady-state entanglement which is quantified by the concurrence of the state proposed by Hill and Wootters [69]. For stronger driving strengths, as can be obtained from the tomography in Figs. 4(b) and 4(d), the system is weakly coherent and is in the maximum

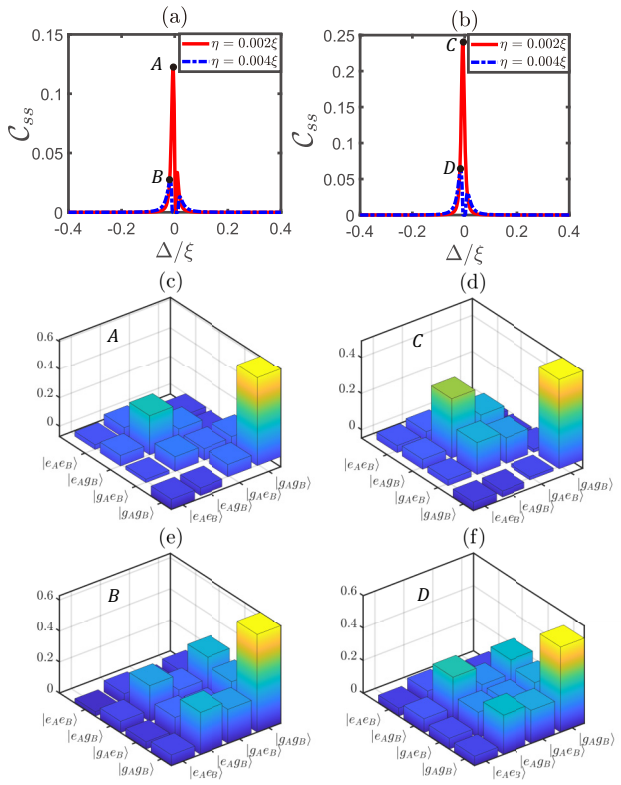

FIG. 5. Concurrence of the steady states for the case (II) in (a) and the case (III) (b). The parameters are set as $\Delta = 0$ and $g = f = 0.05\xi$. Panels (c)–(f) are the tomography of the state at the four black dots in (a) and (b).

mixing state but without entanglement. Therefore, we explore the steady-state entanglement when the driving strength is comparable to the effective coupling strength J. The results for (II) and (III) cases are demonstrated in Figs. 5(a) and 5(b), respectively, under different driving strengths. When the driving strength is $\eta = 0.004\xi$, we find the appearance of the Rabi splitting in both of the cases, which indicates the waveguide induced effective coupling between the two giant atoms. When the driving field is resonant with the frequency difference between the dressed states and the ground state, a relative large entanglement can be achieved and the concurrence peaks locate at $\delta = \pm\sqrt{2}J$. However, when the system is subject to a weakly driven field of $\eta = 0.002\xi$, there are two peaks in case (II) while they are fused into a single one in case (III). This is because the dissipation rate of the giant atom B is $J_2 = 2J$, which is larger than that in case (II) with $J_2 = J$. On the other hand, due to the waveguide induced dissipation, the steady state is a mixed state of the dressed states and the ground state; therefore, the concurrence is much smaller than 1 as shown in Figs. 5(a) and 5(b). To demonstrate the state more clearly, we tomograph the steady states in Figs. 5(c)–5(f). When $\eta = 0.002\xi$, as shown in Figs. 5(c) and 5(d), the probability of being in the dressed state is greater in Fig. 5(d) than that in Fig. 5(c). Correspondingly, the entanglement in Fig. 5(b) is larger than that in Fig. 5(a). Similarly, for $\eta = 0.004\xi$, the greater coherence in case (III) also corresponds to a stronger entanglement.

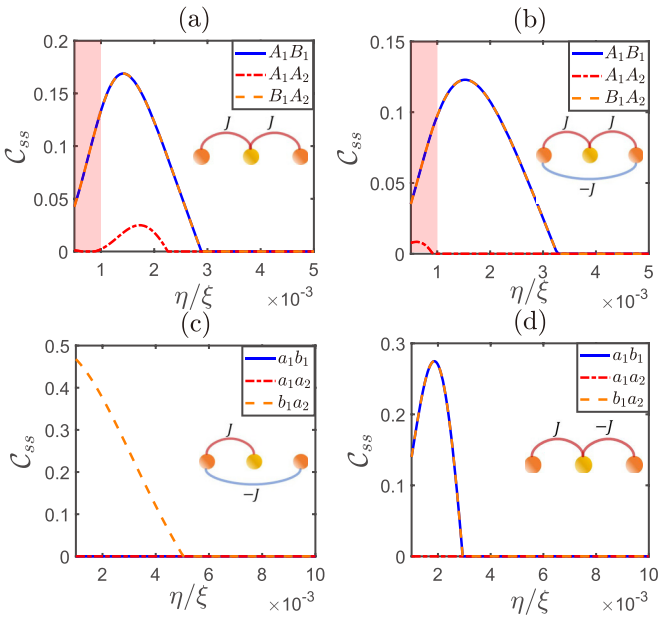

FIG. 6. (a), (b) Steady-state entanglement in the three-giant-atom setting with case (II) and case (III), respectively. (c), (d) The steady-state entanglement of the small-atom setup. The red dashed line gives the results for the next neighbor entanglement as a function of drive strength. The parameters are set as $\Delta = 0$, $g = f = 0.05\xi$.

IV. THREE GIANT ATOMS

To explore the potential application of our proposal with giant atoms in the quantum information processing, we generalize the above discussion to the setup consisting of three giant atoms which are composed of two A type atoms (denoted by A_1 and A_2, respectively) and one B type atom (denoted by B_1). Since the B type atom in case (I) is decoupled with the waveguide, we here constrain ourselves to case (II) and case (III). Then, the master equation for the giant atoms is $\dot{\rho} = -i[\mathcal{H}_i, \rho] + D_i\rho$ $(i = \mathrm{II}, \mathrm{III})$, where the corresponding effective Hamiltonians and the dissipative terms in the rotating frame are respectively

$$\mathcal{H}_{\mathrm{II}} = \Delta(\sigma_z^{(1)} + \sigma_z^{(2)}) + \Delta\Gamma_z^{(1)} + J(\sigma_+^{(1)}\sigma_-^{(1)} + \sigma_+^{(2)}\sigma_-^{(2)}) - J\Gamma_+^{(1)}\Gamma_-^{(1)} + J(\sigma_+^{(1)}\Gamma_-^{(1)} + \Gamma_+^{(1)}\sigma_-^{(2)} + \mathrm{H.c.}), \quad (17)$$

$$D_{\mathrm{II}}\rho = JD_{[\sigma_+^{(1)},\sigma_-^{(1)}]\rho} + JD_{[\sigma_+^{(2)},\sigma_-^{(2)}]\rho} + JD_{[\Gamma_+^{(1)},\Gamma_-^{(1)}]\rho} - J\left(D_{[\sigma_+^{(1)},\sigma_-^{(2)}]\rho} + D_{[\sigma_+^{(2)},\sigma_-^{(1)}]\rho}\right), \quad (18)$$

and

$$\mathcal{H}_{\mathrm{III}} = \Delta\left(\sigma_z^{(1)} + \sigma_z^{(2)}\right) + \Delta\Gamma_z^{(1)} + J(\sigma_+^{(1)}\sigma_-^{(1)} + \sigma_+^{(2)}\sigma_-^{(2)}) + J(\sigma_+^{(1)}\Gamma_-^{(1)} + \Gamma_+^{(1)}\sigma_-^{(2)} - \sigma_+^{(1)}\sigma_-^{(2)} + \mathrm{H.c.}), \quad (19)$$

$$D_{\mathrm{III}}\rho = JD_{[\sigma_+^{(1)},\sigma_-^{(1)}]\rho} + JD_{[\sigma_+^{(2)},\sigma_-^{(2)}]\rho} + 2JD_{[\Gamma_+^{(1)},\Gamma_-^{(1)}]\rho} - J\left(D_{[\sigma_+^{(1)},\Gamma_-^{(1)}]\rho} + D_{[\Gamma_+^{(1)},\sigma_-^{(1)}]\rho}\right) - J\left(D_{[\sigma_+^{(2)},\Gamma_-^{(1)}]\rho} + D_{[\Gamma_+^{(1)},\sigma_-^{(2)}]\rho}\right). \quad (20)$$

In Figs. 6(a) and 6(b), we plot the two atom steady-state entanglement as a function of the drive strength for cases (II) and (III), respectively. Correspondingly, the waveguide induced effective atomic couplings are demonstrated in the inset. In both cases, the entanglements between the neighbor atoms (A_1B_1 and B_1A_2) agree with each other and are larger than that of the next neighbor ones. The difference is reflected in the next neighbor atomic entanglement. For the weak driving, a more pronounced next neighbor entanglement can be generated in case (III) as shown in the shaded regime of Figs. 6(a) and 6(b). The significant difference stems from the waveguide induced atomic coupling. In case (II), there is only the neighbor atomic coupling with strength J. For case (III), we further find the next neighbor atomic coupling with strength $-J$ and it forms a cyclic coupling. Therefore, compared to case (II), there is more next neighbor atomic entanglement in case (III). When the driving strength is further increased to be greater than the effective coupling strength induced by the waveguide, the neighbor entanglement vanishes so that the system is in a maximally mixed state, which is consistent with the discussion in Figs. 4 and 5.

As a comparison, we also discuss the steady-state entanglement when an array of small atoms couple to the waveguide via a single coupling site for each atom. Here, we consider that two neighboring small atoms (labeled a and b) constitute a unit cell, with both the intracell and extra-cell atomic distances being adjustable on demand. The Hamiltonian of the small atom setup and the master equation is given in Appendix B. There exist two coupling cases which are listed in Fig. 10. Correspondingly, the steady-state concurrence as a function of the driving strength and the effective interatom coupling is plotted in Figs. 6(c) and 6(d). It shows that, for both of the two cases, the next neighbor atomic entanglement is always zero, due to the absence of the cyclic coupling configuration.

V. ENTANGLEMENT MANIPULATION BY ARTIFICIAL MAGNETIC FIELD

In the above section, we find an intriguing phenomena that the giant atom system will generate the atomic entanglement even between the next neighbor atom pairs. It is natural to further explore how to manipulate the degree of entanglement. One approach is to induce the phase in the driven field, which serves as the artificial magnetic fields [63–66]. Due to the cyclic coupling, the phase difference between different atoms cannot be eliminated by any gauge transformation. Therefore, we write the driving Hamiltonian in the rotating frame as

$$H_d = \sum_{n,m}\eta(\sigma_+^{(n)} + \Gamma_+^{(m)}e^{-i\phi} + \mathrm{H.c.}), \quad (21)$$

with the strength η and the phase ϕ. Phenomenally, we approximate that the other parts in the effective Hamiltonian and the master equation are not changed by the phase ϕ.

We begin with the two atom setup, where the modulation of entanglement via the artificial magnetic field (the driving phase cannot be eliminated by canonical transformation) is demonstrated in Fig. 7 for both giant- and small-atom configurations. A general result is that the modulation to the giant atomic configuration is more obvious than that to the small

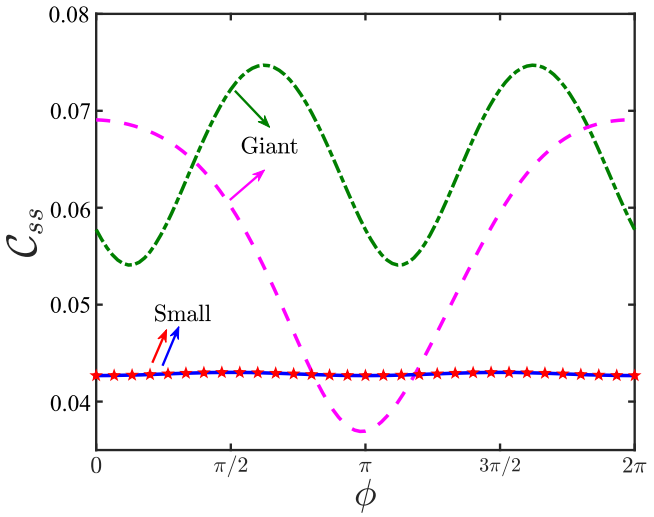

FIG. 7. Steady-state entanglement modulated by artificial magnetic field for the case of the giant atoms and the small atoms. The green dashed line and purple dashed line correspond to case (II) and case (III) geometric configurations in the giant-atom configuration, respectively. The blue solid line and red star line represent the results for small atoms. The parameters are set as $\Delta = 0$, $g = f = 0.06\xi$, and $\eta = 0.002\xi$.

atoms. Therefore, the giant-atom system provides us with an approach to tune the entanglement with a wider regime via the artificial magnetic field. As we have already discussed in Sec. III, the effective coupling of the two giant atoms is the same in cases (II) and (III). However, the presence of the larger individual dissipation of the B atom in case (III) with $J_2 = 2J$ makes the concurrence decrease rapidly with the modulation of the driving phase, as shown by the purple dashed line in Fig. 7. Furthermore, the two cases listed in Fig. 10 for two small atoms are the same with each other; therefore, the curves for the small atoms coincide with each other. Case (II) in the giant-atom configurations has the similar form as in the small-atom configurations, as listed in Fig. 2 and Fig. 10. Therefore, the significant difference in the modulation is originated from the waveguide-induced Lamb shift of the giant atoms, which is not achievable in the small-atom configurations.

Next, let us move to the system with three atoms and compare the steady-state entanglement between the giant- and small-atoms setups. In the upper panel of Figs. 8(a)–8(d), we illustrate the entanglement for cases (II), (III) in the giant-atom setups and cases (I), (II) in the small-atom setups and the corresponding energy-level diagrams are also given in the lower panel. In the energy diagram, we define the states $|\psi_{\mathrm{A(a)_I}}\rangle = |e, g, g\rangle$, $|\psi_{\mathrm{B(b)_I}}\rangle = |g, e, g\rangle$, $|\psi_{\mathrm{A(a)_2}}\rangle = |g, g, e\rangle$, and $|\psi_0\rangle = |g, g, g\rangle$. Here, the capital letters A and B represent the giant atoms while the lowercase letters a and b represent the small atoms. The blue (green) solid arrows represent the driving field (waveguide) induced transitions and the yellow dashed arrows are the waveguide induced atomic collective dissipations.

We first discuss the setup with three giant atoms, in which both the neighbor atomic entanglement $[\mathcal{C}_{ss}(A_1B_1) = \mathcal{C}_{ss}(B_1A_2)]$ and the next neighbor atomic entanglement $[\mathcal{C}_{ss}(A_1A_2)]$ can be effectively modulated by the artificial magnetic field. This can be explained by the cyclic energy diagram

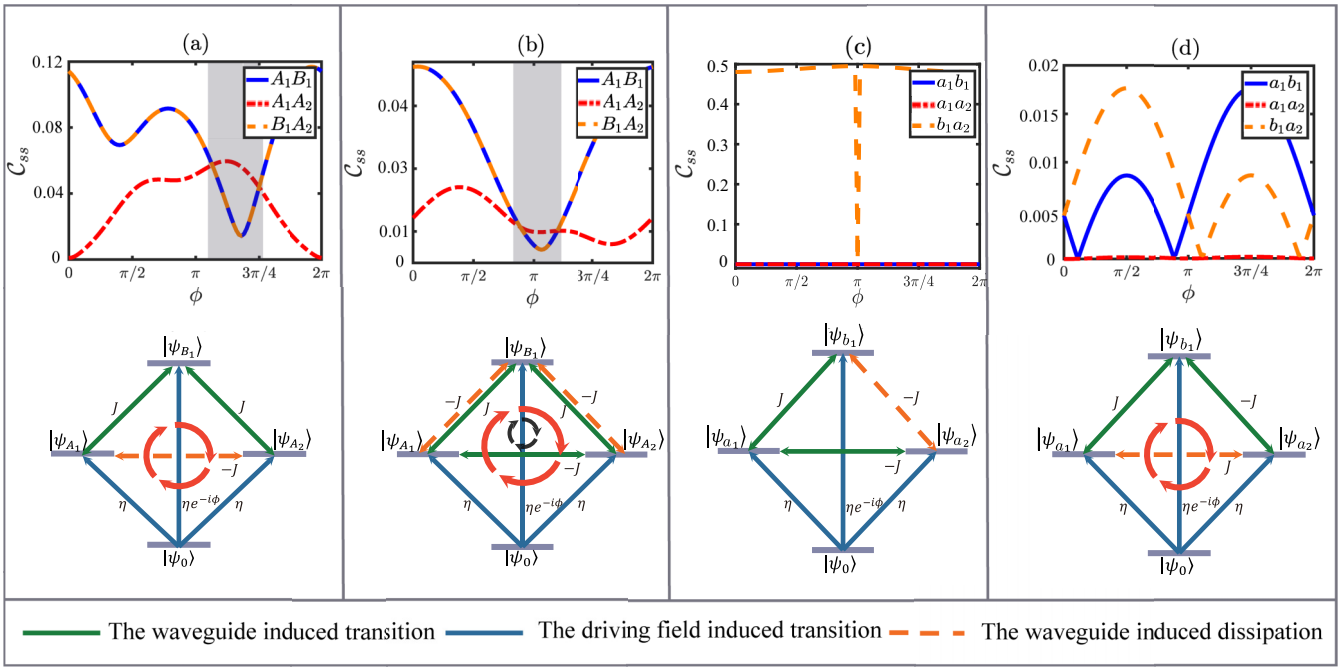

FIG. 8. Steady-state entanglement modulated by an artificial magnetic field for the case of the giant atoms (a), (b) and the small atoms (c), (d). The red dashed line represents the next neighbor entanglement. The blue solid line and orange dashed line represent the neighbor entanglement. The parameters are set as $\Delta = 0$, $g = f = 0.08\xi$, and $\eta = 0.002\xi$. The lower part is the diagram of the energy levels corresponding to the geometric configuration. The blue line represents the extra driving field, the green line represents the atomic coupling induced by the waveguide, and the yellow dashed line represents the associated dissipation.

as shown in the lower panel of Figs. 8(a) and 8(b). For case (II) represented by Fig. 8(a), the presence of the driving field leads to the cyclic diagram to the system. For case (III), we can also observe the $|\psi_{A_1}\rangle \to |\psi_{B_1}\rangle \to |\psi_{A_2}\rangle \to |\psi_0\rangle$ cycle which is the same as case (II). Furthermore, there exists another $|\psi_{A_1}\rangle \to |\psi_{B_1}\rangle \to |\psi_{A_2}\rangle$ cycle which is induced only by the waveguide induced atomic coupling and is denoted by the black circle in the lower panel of Fig. 8(b). Due to these cyclic transitions, the atomic entanglement can be significantly modulated by the artificial magnetic field and even the next neighbor entanglement can surpass those of neighbor ones, which is exhibited in the shaded regime of the upper panel of Figs. 8(a) and 8(b). It is worth noting that the next neighbor entanglement in Fig. 8(b) is smaller than that in Fig. 8(a). This is due to the weakened role of the black closed cycle constituted by the waveguide interactions in Fig. 8(b).

The results for three small-atom setups are given in Figs. 8(c) and 8(d) for cases (I) and (II), respectively. Here, the cyclic transition $|\psi_{A_1}\rangle \to |\psi_{B_1}\rangle \to |\psi_{A_2}\rangle \to |\psi_0\rangle$ is formed in case (II) [as shown in Fig. 8(d)] but not in case (I) [as shown in Fig. 8(c)]. Therefore, the next neighbor entanglement is always zero in the latter case but can be manipulated by the artificial magnetic field in the former case.

Combining the four cases, only the presence of the red closed cycle in Fig. 8 allows the manipulation of next neighbor entanglement. Comparing Figs. 8(b) and 8(c), the closed cycles containing neighbor atoms are all present ($|\psi_{A_1}\rangle \to |\psi_{A_2}\rangle \to |\psi_0\rangle$), but the absence of the red closed cycle makes manipulation of the next neighbor entanglement in Fig. 8(c) impossible. One should also note that the $-J$ for $|\psi_{b_1}\rangle \to |\psi_{a_2}\rangle$ transition in Fig. 8(d) instead of the J for $|\psi_{B_1}\rangle \to |\psi_{A_2}\rangle$ transition in Fig. 8(a) results in modulation of the next neighbor entanglement being not significant in Fig. 8(d). On the other hand, in the small-atoms cases, the next neighbor entanglement is not only smaller than the counterpart in the giant atom but also smaller than the neighbor ones. Therefore, the giant-atom system is of great potential to obtain and manipulate the atomic entanglement.

VI. CONCLUSION

In this paper, we have proposed a scheme to realize the controllable coupling and collective dissipation among the giant atoms, which is mediated by the coupled resonator waveguide. In the microwave regime, the working frequency transmission line resonator is in the order of GHz; the photonic hopping strength between the neighbor site ξ can achieve hundreds of MHz [70,71]. With the platform of superconducting materials, the controllable coupled resonator waveguide has also been realized by the high-impedance microwave resonators and, by expanding the capacitively coupled lumped element, the nearest hopping strength has been achieved from 50 MHz to 200 MHz [72–74]. The giant atom was initially realized at the surface acoustic wave platform by coupling a superconducting transmon quantum qubit [4]. With the development in microwave superconducting materials, the giant atom was also achieved by coupling artificial atoms made of Josephson junctions into superconducting circuits through capacitance or inductance. In such systems, the coupling strength g is much smaller than the hopping strength ξ with the existing technology [75–77].

In conclusion, we have investigated the engineering of the interaction and entanglement among the driven giant atoms via tuning of their geometric configurations. By adjusting the artificial magnetic field, the next neighbor atomic entanglement can be further enhanced and is expected to surpass the neighbor ones in the giant-atoms system in principle. This entanglement is limited by the fact that the waveguide induced dissipation is in the same order of magnitude as the effective coupling strength. Actually, both the neighbor and next neighbor atomic entanglement is hopefully enhanced with the assistance of some strategies, for example, to induce the direct atomic interaction or designing the giant-atom array system to support strong entanglement via the quantum phase transition, etc. Since the giant-atom setup is mainly realized in superconducting circuits, which are widely used to design kinds of coupling schemes, these proposals are potentially achievable in experiment. This next neighbor atomic enhancement is not found in the small-atom setup and it is expected that it will be useful in constructing the quantum network and realizing quantum information processing.

ACKNOWLEDGMENTS

Z.W. is supported by the Science and Technology Development Project of Jilin Province (Grant No. 20230101357JC) and the National Science Foundation of China (Grant No. 12375010). X.W. is supported by the National Natural Science Foundation of China (NSFC; Grants No. 12174303 and No. 11804270) and the Fundamental Research Funds for the Central Universities (Grant No. xzy012023053).

APPENDIX A: MASTER EQUATION FOR GIANT-ATOM SETUP

In this Appendix, we outline the derivation of the master equation (7), which governs the dynamics of the system by considering the coupling resonator waveguide as the environment. In the interaction picture, the interaction Hamiltonian can be rewritten as follows:

$$H_I = g\sum_n [\sigma_+^{(n)} E(A_n,t)e^{i\Omega t} + \text{H.c.}] + f\sum_m [\Gamma_+^{(m)} E(B_m,t)e^{i\Omega t} + \text{H.c.}], \tag{A1}$$

where

$$E(A_n,t) = \frac{1}{\sqrt{N_c}}\sum_{k,n} a_k e^{-i\omega_k t}(e^{ikx_n} + e^{ik(x_n+t_A)}),$$
$$E(B_m,t) = \frac{1}{\sqrt{N_c}}\sum_{k,m} a_k e^{-i\omega_k t}(e^{iky_m} + e^{ik(y_m+t_B)}). \tag{A2}$$

Under the Markov approximation and in the interaction picture, the formal master equation for the quantum open system reads [68]

$$\dot{\rho}(t) = -\int_0^\infty d\tau\, \text{Tr}_c\{[H_I(t),[H_I(t-\tau),\rho_c\otimes\rho(t)]]\}. \tag{A3}$$

Since we are working at zero temperature, the waveguide is in its vacuum state initially. Therefore, we will have $\mathrm{Tr}_c[E^\dagger(X,t)E(X,t-\tau)\rho_c]=0$. Back to the Schrödinger picture, the above equation becomes

$$\begin{aligned}\dot{\rho}=&\sum_n\sum_m\Big\{-i\Big[\frac{\Omega}{2}\sigma_z^n+\frac{\Omega}{2}\Gamma_z^m,\rho\Big]\\&+(A_{11}+A_{11}^*)\sigma_-^n\rho\sigma_+^m-A_{11}\sigma_+^n\sigma_-^m\rho-A_{11}^*\rho\sigma_+^n\sigma_-^m\\&+(A_{22}+A_{22}^*)\Gamma_-^n\rho\Gamma_+^m-A_{22}\Gamma_+^n\Gamma_-^m\rho-A_{22}^*\rho\Gamma_+^n\Gamma_-^m\\&+(A_{12}+A_{12}^*)\sigma_-^n\rho\Gamma_+^m-A_{12}\sigma_+^n\Gamma_-^m\rho-A_{12}^*\rho\sigma_+^n\Gamma_-^m\\&+(A_{21}+A_{21}^*)\Gamma_-^n\rho\sigma_+^m-A_{21}\Gamma_+^n\sigma_-^m\rho-A_{21}^*\rho\Gamma_+^n\sigma_-^m\Big\},\end{aligned}\tag{A4}$$

where

$$\begin{aligned}A_{11}&=g^2\int_0^\infty d\tau\,e^{i\Omega\tau}\mathrm{Tr}_c\Big(\sum_n\sum_m E(A_n,t)E^\dagger(A_m,t-\tau)\rho_c\Big)\\&=g^2\sum_n\sum_m\int_0^\infty d\tau\,e^{i\Omega\tau}\mathrm{Tr}_c\{[(E(x_n,t)+E(x_n+t_A,t))\\&\quad\times(E^\dagger(x_m,t-\tau)+E^\dagger(x_m+t_A,t-\tau))]\rho_c\}\\&=g^2\sum_n\sum_m\int_0^\infty d\tau\,e^{i\Omega\tau}\mathrm{Tr}_c[E(x_n,t)E^\dagger(x_m,t-\tau)\rho_c\\&\quad+E(x_n,t)E^\dagger(x_m+t_A,t-\tau)\rho_c\\&\quad+E(x_n+t_A,t)E^\dagger(x_m,t-\tau)\rho_c\\&\quad+E(x_n+t_A,t)E^\dagger(x_m+t_A,t-\tau)\rho_c].\end{aligned}\tag{A5}$$

We can see that the integral in the above equation involves four terms. Let us take one of them for example to show our calculation. The first term of the above equation is [67]

$$\begin{aligned}&\sum_n\sum_m\int_0^\infty d\tau\,e^{i\Omega\tau}\mathrm{Tr}_c[E(x_n,t)E^\dagger(x_m,t-\tau)\rho_c]\\&=\sum_n\sum_m\int_0^\infty d\tau\frac{e^{i\Omega\tau}}{N_c}\\&\quad\times\mathrm{Tr}\Big[\sum_{k,k'}e^{-i\omega_k t}e^{ikx_n}a_k e^{i\omega_{k'}(t-\tau)}e^{-ik'x_m}a_{k'}^\dagger\rho_c\Big]\\&=\sum_n\sum_m\int_0^\infty\frac{d\tau}{N_c}\sum_k[e^{-i(\omega_k-\Omega)\tau}e^{-ik(x_m-x_n)}]\\&=\sum_n\sum_m\int_0^\infty\frac{d\tau}{N_c}\sum_{n=0}^{N_c-1}e^{-i\Delta_c\tau}e^{\frac{-2\pi i(x_m-x_n)n_c}{N_c}}e^{2i\xi\,\cos(\frac{2\pi n_c}{N_c})\tau}\\&=\sum_n\sum_m\int_0^\infty d\tau\frac{e^{-i\Delta_c\tau}}{N_c}\sum_{n=0}^{N_c-1}e^{\frac{-2\pi i(x_m-x_n)n_c}{N_c}}\\&\quad\times\sum_{j=-\infty}^{\infty}i^jJ_j(2\xi\tau)e^{i2\pi n_c j/N_c}\\&=\sum_n\sum_m\int_0^\infty d\tau\,e^{-i\Delta_c\tau}i^{|x_n-x_m|}J_{|x_n-x_m|}(2\xi\tau)\\&=\sum_n\sum_m\frac{1}{2\xi}e^{i\frac{\pi}{2}|x_n-x_m|}.\end{aligned}\tag{A6}$$

In the above calculations,we have considered that the giant atom is resonant with the bare resonator ($\Delta_c=\omega_c-\Omega=0$) and apply the formula

$$\int_0^\infty d\tau\,J_j(a\tau)=\frac{1}{|a|}.\tag{A7}$$

Therefore, we will finally achieve $A_{ij}=\sum_{n,m}A_{ij}^{(n,m)}$, where

$$A_{11}^{(n,m)}=\frac{1}{2\xi}(2\,e^{i\frac{\pi}{2}|x_n-x_m|}+e^{i\frac{\pi}{2}|x_n-x_m-t_A|}+e^{i\frac{\pi}{2}|x_n+t_A-x_m|}).\tag{A8}$$

$$A_{22}^{(n,m)}=\frac{1}{2\xi}(2\,e^{i\frac{\pi}{2}|y_n-y_m|}+e^{i\frac{\pi}{2}|y_n-y_m-t_B|}+e^{i\frac{\pi}{2}|y_n+t_B-y_m|}).\tag{A9}$$

$$\begin{aligned}A_{12}^{(n,m)}=\frac{1}{2\xi}&(e^{i\frac{\pi}{2}|x_n-y_m|}+e^{i\frac{\pi}{2}|x_n-y_m-t_B|}\\&+e^{i\frac{\pi}{2}|x_n+t_A-y_m|}+e^{i\frac{\pi}{2}|x_n+t_A-y_m-t_B|}),\end{aligned}\tag{A10}$$

$$\begin{aligned}A_{21}^{(n,m)}=\frac{1}{2\xi}&(e^{i\frac{\pi}{2}|y_n-x_m|}+e^{i\frac{\pi}{2}|y_n-x_m-t_A|}\\&+e^{i\frac{\pi}{2}|y_n+t_B-x_m|}+e^{i\frac{\pi}{2}|y_n+t_B-x_m-t_A|}).\end{aligned}\tag{A11}$$

After regrouping the terms, we will get the final form which is given in Eq. (12) of the main text.

APPENDIX B: MASTER EQUATION FOR SMALL-ATOM SETUP

In the main text, we compare and discuss the configuration of giant atoms with that of small atoms. Here, we provide a specific model and master equation form for the considered small-atom configuration and briefly discuss them. Similarly, we consider the interaction between a small atomic array composed of two-level atoms and a one-dimensional coupled-resonator waveguide. We consider the array composed of small atoms, where two neighboring small atoms form a protocell, labeled a and b, respectively, with different inter- and extra-cell atomic distance which can be adjusted, sketched in Fig. 9. Giant atoms can be coupled to the waveguide through multiple sites, while each small atom can only be coupled to the waveguide via only one site. In the small-atom configuration, the Hamiltonian of the system is written as

$$H_c=\omega_c\sum_j a_j^\dagger a_j-\xi\sum_j(a_{j+1}^\dagger a_j+a_j^\dagger a_{j+1}),\tag{B1}$$

$$\begin{aligned}H=H_c+\frac{\Omega}{2}\sum_n\nu_z^{(n)}+\frac{\Omega}{2}\sum_m\tau_z^{(m)}\\+\sum_{n,m}\big[g a_{x_n}^\dagger\nu_-^{(n)}+f a_{y_m}^\dagger\tau_-^{(m)}+\mathrm{H.c.}\big].\end{aligned}\tag{B2}$$

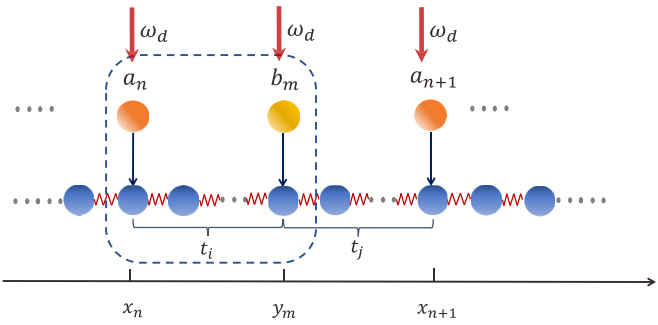

FIG. 9. Small atoms coupled to a 1D coupled-resonator waveguide. We label the odd number of small atoms as a (orange ball) and the even number of small atoms as b (yellow ball).

Here, x_n and y_m are the coupling site between the small atoms and the one-dimensional coupled-resonator waveguide. The parameters t_i, t_j are the intracell atomic distance and the extracell atomic distance, respectively. After the same derivation process, we can obtain the master equation for small atoms:

$$\begin{aligned}\dot{\rho} = &-i[\mathcal{H}, \rho] \\ &+\sum_{n,m}[g^2 U_{11}^{(n,m)}(2\nu_-^{(n)}\rho\nu_+^{(m)} - \nu_+^{(m)}\nu_-^{(n)}\rho - \rho\nu_+^{(n)}\nu_-^{(m)}) \\ &+f^2 U_{22}^{(n,m)}(2\tau_-^{(n)}\rho\tau_+^{(m)} - \tau_+^{(n)}\tau_-^{(m)}\rho - \rho\tau_+^{(n)}\tau_-^{(m)}) \\ &+gf U_{12}^{(n,m)}(2\nu_-^{(n)}\rho\tau_+^{(m)} - \nu_+^{(n)}\tau_-^{(m)}\rho - \rho\nu_+^{(n)}\tau_-^{(m)}) \\ &+gf U_{21}^{(n,m)}(2\tau_-^{(n)}\rho\nu_+^{(m)} - \tau_+^{(n)}\nu_-^{(m)}\rho - \rho\tau_+^{(n)}\nu_-^{(m)})],\end{aligned} \tag{B3}$$

where the coherent coupling between the atoms is

$$\begin{aligned}\mathcal{H} = &\sum_{n,m}\left(\frac{\Omega}{2}\nu_z^{(n)} + \frac{\Omega}{2}\tau_z^{(m)}\right) \\ &+\sum_{n,m}[g^2 I_{11}\nu_+^{(n)}\nu_-^{(m)} + f^2 I_{22}\tau_+^{(n)}\tau_-^{(m)}] \\ &+\sum_{n,m}[gf(I_{12}\nu_+^{(n)}\tau_-^{(m)} + I_{21}\tau_+^{(n)}\nu_-^{(m)})].\end{aligned} \tag{B4}$$

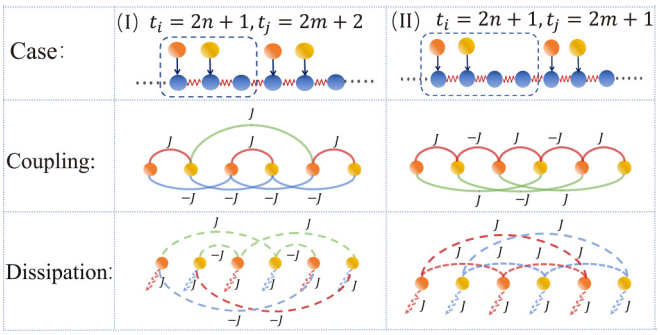

FIG. 10. Effective couplings and dissipations for two different cases. The first line is the simple illustration of different systems. The second line is a schematic diagram of the corresponding effective coherent interaction. The last line shows the diagram of effective dissipation.

In the above equations, we have defined $U_{ij} = \sum_{n,m}\mathrm{Re}(A_{ij}^{(n,m)})$, $I_{ij} = \sum_{m,n}\mathrm{Im}(A_{ij}^{(n,m)})(i, j = 1, 2)$, where

$$\begin{aligned}A_{11}^{(n,m)} &= \frac{1}{2\xi}e^{i\frac{\pi}{2}|x_n - x_m|}, \\ A_{11}^{(n,m)} &= \frac{1}{2\xi}e^{i\frac{\pi}{2}|y_n - y_m|}, \\ A_{12}^{(n,m)} &= A_{21}^{(n,m)} = \frac{1}{2\xi}e^{i\frac{\pi}{2}|x_n - y_m|}.\end{aligned} \tag{B5}$$

The form of interaction between small atoms is also related to the spacing between them. For convenience, we fix the intracellular distance as $t_i = 1$. By changing the intercellular distance t_j, we find that there are two cases of interactions for small atoms, as shown in Fig. 10. We present the geometric configurations of two cases of interaction and their corresponding associated dissipation. For the two small-atom configurations, it can be visually seen from Fig. 10 that there is no cyclic coupling structure as the giant-atom configuration.

With the two atoms setup, the master equation for the (I) and (II) cases becomes

$$\dot{\rho} = -i[\mathcal{H}_\mathrm{I} + H_d, \rho] + JD_{[\nu_+,\nu_-]\rho} + JD_{[\tau_+,\Gamma_-]\rho}, \tag{B6}$$

$$\mathcal{H}_\mathrm{I} = \Delta\nu_z + \Delta\Gamma_z + J(\nu_+\tau_- + \tau_+\nu_-) \tag{B7}$$

and

$$\dot{\rho} = -i[\mathcal{H}_\mathrm{II} + H_d, \rho] + JD_{[\nu_+,\nu_-]\rho} + JD_{[\tau_+,\tau_-]\rho}, \tag{B8}$$

$$\mathcal{H}_\mathrm{II} = \Delta\nu_z + \Delta\tau_z + J(\nu_+\tau_- + \tau_+\nu_-), \tag{B9}$$

where $\mathcal{H}$ is the effective Hamiltonian and $D_{[O_1,O_2]\rho} = 2O_2\rho O_1 - \rho O_1 O_2 - O_1 O_2\rho$. In the rotating frame, the driving Hamiltonian is written as $H_d = \eta(\nu_+ + \tau_+ + \mathrm{H.c.})$.

The master equation for the three atoms setup is $\dot{\rho} = -i[\mathcal{H}_i, \rho] + D_i\rho\,(i = \mathrm{I}, \mathrm{II})$, where the corresponding effective Hamiltonians and the dissipators in the rotating frame are respectively

$$\begin{aligned}\mathcal{H}_\mathrm{I} = &\Delta\left(\nu_z^{(1)} + \nu_z^{(2)}\right) + \Delta\tau_z^{(1)} \\ &+(J\nu_+^{(1)}\tau_-^{(1)} - J\nu_+^{(1)}\nu_-^{(2)} + \mathrm{H.c.}),\end{aligned} \tag{B10}$$

$$\begin{aligned}D_\mathrm{I}\rho = &JD_{[\nu_+^{(1)},\nu_-^{(1)}]\rho} + JD_{[\nu_+^{(2)},\nu_-^{(2)}]\rho} + JD_{[\tau_+^{(1)},\tau_-^{(1)}]\rho} \\ &-J(D_{[\tau_+^{(1)},\nu_-^{(2)}]\rho} + D_{[\nu_+^{(2)},\tau_-^{(1)}]\rho})\end{aligned} \tag{B11}$$

and

$$\begin{aligned}\mathcal{H}_\mathrm{II} = &\Delta\left(\nu_z^{(1)} + \nu_z^{(2)}\right) + \Delta\tau_z^{(1)} \\ &+(J\nu_+^{(1)}\tau_-^{(1)} - J\tau_+^{(1)}\nu_-^{(2)} + \mathrm{H.c.}),\end{aligned} \tag{B12}$$

$$\begin{aligned}D_\mathrm{II}\rho = &JD_{[\nu_+^{(1)},\nu_-^{(1)}]\rho} + JD_{[\nu_+^{(2)},\nu_-^{(2)}]\rho} + JD_{[\tau_+^{(1)},\tau_-^{(1)}]\rho} \\ &-J(D_{[\nu_+^{(1)},\nu_-^{(2)}]\rho} + D_{[\nu_+^{(2)},\nu_-^{(1)}]\rho}).\end{aligned} \tag{B13}$$

[1] P. Forn-Díaz, L. Lamata, E. Rico, J. Kono, and E. Solano, Rev. Mod. Phys. **91**, 025005 (2019).

[2] R. Gutzler, M. Garg, C. R. Ast, K. Kuhnke, and K. Kern, Nat. Rev. Phys. **3**, 441 (2021).

[3] D. F. Walls and G. J. Milburn, *Quantum Optics*, 2nd ed. (Springer, Berlin, 2008).

[4] M. V. Gustafsson, T. Aref, A. F. Kockum, M. K. Ekström, G. Johansson, and P. Delsing, Science **346**, 207 (2014).

[5] A. Frisk Kockum, P. Delsing, and G. Johansson, Phys. Rev. A **90**, 013837 (2014).

[6] R. Manenti, A. F. Kockum, A. Patterson, T. Behrle, J. Rahamim, G. Tancredi, F. Nori, and P. J. Leek, Nat. Commun. **8**, 975 (2017).

[7] A. Noguchi, R. Yamazaki, Y. Tabuchi, and Y. Nakamura, Phys. Rev. Lett. **119**, 180505 (2017).

[8] K. J. Satzinger, Y. P. Zhong, H.-S. Chang, G. A. Peairs, A. Bienfait, M.-H. Chou, A. Y. Cleland, C. R. Conner, E. Dumur, J. Grebel, I. Gutierrez, B. H. November, R. G. Povey, S. J. Whiteley, D. D. Awschalom, D. I. Schuster, and A. N. Cleland, Nature (London) **563**, 661 (2018).

[9] A. Ask, M. Ekström, P. Delsing, and G. Johansson, Phys. Rev. A **99**, 013840 (2019).

[10] A. F. Kockum, Quantum optics with giant atoms the first five years, in *Mathematics for Industry* (Springer, Singapore, 2021), pp. 125–146.

[11] B. Kannan, M. Ruckriegel, D. Campbell, A. F. Kockum, J. Braumüller, D. Kim, M. Kjaergaard, P. Krantz, A. Melville, B. M. Niedzielski, A. Vepsäläinen, R. Winik, J. Yoder, F. Nori, T. P. Orlando, S. Gustavsson, and W. D. Oliver, Nature (London) **583**, 775 (2020).

[12] Y. T. Chen, L. Du, L. Guo, Z. Wang, Y. Zhang, Y. Li, and J. H. Wu, Commun. Phys. **5**, 215 (2022).

[13] X.-L. Yin, Y.-H. Liu, J.-F. Huang, and J.-Q. Liao, Phys. Rev. A **106**, 013715 (2022).

[14] L. Guo, A. L. Grimsmo, A. F. Kockum, M. Pletyukhov, and G. Johansson, Phys. Rev. A **95**, 053821 (2017).

[15] L. Du, M. R. Cai, J. H. Wu, Z. Wang, and Y. Li, Phys. Rev. A **103**, 053701 (2021).

[16] Q.-Y. Qiu, Y. Wu, and X.-Y. Lu, Sci. China Phys. Mech. Astron. **66**, 224212 (2023).

[17] L. Guo, A. F. Kockum, F. Marquardt, and G. Johansson, Phys. Rev. Res. **2**, 043014 (2020).

[18] W. Zhao and Z. Wang, Phys. Rev. A **101**, 053855 (2020).

[19] X. Wang, T. Liu, A. F. Kockum, H.-R. Li, and F. Nori, Phys. Rev. Lett. **126**, 043602 (2021).

[20] W. Cheng, Z. Wang, and Y.-X. Liu, Phys. Rev. A **106**, 033522 (2022).

[21] K. H. Lim, W.-K. Mok, and L.-C. Kwek, Phys. Rev. A **107**, 023716 (2023).

[22] G. Andersson, B. Suri, L. Guo, T. Aref, and P. Delsing, Nat. Phys. **15**, 1123 (2019).

[23] S. Guo, Y. Wang, T. Purdy, and J. Taylor, Phys. Rev. A **102**, 033706 (2020).

[24] X.-L. Yin, W.-B. Luo, and J.-Q. Liao, Phys. Rev. A **106**, 063703 (2022).

[25] L. Du, L. Guo, and Y. Li, Phys. Rev. A **107**, 023705 (2023).

[26] X. Zhang, C. Liu, Z. Gong, and Z. Wang, Phys. Rev. A **108**, 013704 (2023).

[27] A. F. Kockum, G. Johansson, and F. Nori, Phys. Rev. Lett. **120**, 140404 (2018).

[28] A. Carollo, D. Cilluffo, and F. Ciccarello, Phys. Rev. Res. **2**, 043184 (2020).

[29] X. Wang and H.-R. Li, Quantum Sci. Technol. **7**, 035007 (2022).

[30] C. Joshi, F. Yang, and M. Mirhosseini, Phys. Rev. X **13**, 021039 (2023).

[31] X. Wang, J.-Q Li, Z. Wang, A. F. Kockum, L. Du, T. Liu, and F. Nori, arXiv:2404.09829.

[32] P.Y. Wen, K.-T. Lin, A.F. Kockum, B. Suri, H. Ian, J.C. Chen, S.Y. Mao, C.C. Chiu, P. Delsing, F. Nori, G.-D. Lin, and I.-C. Hoi, Phys. Rev. Lett. **123**, 233602 (2019).

[33] A. M. Vadiraj, A. Ask, T. G. McConkey, I. Nsanzineza, C. W. S. Chang, A. F. Kockum, and C. M. Wilson, Phys. Rev. A **103**, 023710 (2021).

[34] S. Longhi, Opt. Lett. **45**, 3017 (2020).

[35] Z. Q. Wang, Y. P. Wang, J. Yao, R. C. Shen, W. J. Wu, J. Qian, J. Li, S. Y. Zhu, and J. Q. You, Nat. Commun. **13**, 7580 (2022).

[36] A. González-Tudela, C. S. Munoz, and J. I. Cirac, Phys. Rev. Lett. **122**, 203603 (2019).

[37] L. Du, Y. Zhang, J.-H. Wu, A. F. Kockum, and Y. Li, Phys. Rev. Lett. **128**, 223602 (2022).

[38] H. Xiao, L. Wang, Z.-H. Li, X. Chen, and L. Yuan, npj Quantum Inf. **8**, 80 (2022).

[39] X. Wang, H.-B. Zhu, T. Liu, and F. Nori, Phys. Rev. Res. **6**, 013279 (2024).

[40] A. Soro, C. S. Muñoz, and A. F. Kockum, Phys. Rev. A **107**, 013710 (2023).

[41] S. L. Feng and W. Z. Jia, Phys. Rev. A **104**, 063712 (2021).

[42] A. Soro and A. F. Kockum, Phys. Rev. A **105**, 023712 (2022).

[43] E. R. Ingelsten, A. F. Kockum, and A. Soro, arXiv:2402.10879.

[44] L. Leonforte, X. Sun, D. Valenti, B. Spagnolo, F. Illuminati, A. Carollo, and F. Ciccarello, arXiv:2402.10275.

[45] D. Cilluffo, A. Carollo, S. Lorenzo, J. A. Gross, G. M. Palma, and F. Ciccarello, Phys. Rev. Res. **2**, 043070 (2020).

[46] Q. Y. Cai and W. Z. Jia, Phys. Rev. A **104**, 033710 (2021).

[47] H. Yu, Z. Wang, and J.-H. Wu, Phys. Rev. A **104**, 013720 (2021).

[48] D. D. Noachtar, J. Knorzer, and R. H. Jonsson, Phys. Rev. A **106**, 013702 (2022).

[49] A. C. Santos and R. Bachelard, Phys. Rev. Lett. **130**, 053601 (2023).

[50] L. M. Sieberer, S. D. Huber, E. Altman, and S. Diehl, Phys. Rev. Lett. **110**, 195301 (2013).

[51] T. Leleu, Y. Yamamoto, S. Utsunomiya, and K. Aihara, Phys. Rev. E **95**, 022118 (2017).

[52] T. Fink, A. Schade, S. Höfling, C. Scheider, and A. Imamoglu, Nat. Phys. **14**, 365 (2018).

[53] F. Minganti, A. Biella, N. Bartolo, and C. Ciuti, Phys. Rev. A **98**, 042118 (2018).

[54] L. R. Bakker, M. S. Bahovadinov, D. V. Kurlov, V. Gritsev, A. K. Fedorov, and D. O. Krimer, Phys. Rev. Lett. **129**, 250401 (2022).

[55] N. Pernet, P. St-Jean, D. D. Solnyshkov, G. Malpuech, N. C. Zambon, Q. Fontaine, B. Real, O. Jamadi, A. Lemaitre, M. Morassi, L. L. Gratiet, T. Baptiste, A. Harouri, I. Sagnes, A. Amo, S. Ravets, and J. Bloch, Nat. Phys. **18**, 678 (2022).

[56] J. Agustí, Y. Minoguchi, J. M. Fink, and P. Rabl, Phys. Rev. A **105**, 062454 (2022).

[57] J. Agustí, X. H. H. Zhang, Y. Minoguchi, and P. Rabl, Phys. Rev. Lett. **131**, 250801 (2023).

[58] X.-L. Yin and J.-Q. Liao, Phys. Rev. A **108**, 023728 (2023).
[59] W.-B. Luo, X.-L. Yin, and J.-Q. Liao, Adv. Quantum Technol. **7**, 2400030 (2024).
[60] M. Aidelsburger, M. Atala, M. Lohse, J. T. Barreiro, B. Paredes, and I. Bloch, Phys. Rev. Lett. **111**, 185301 (2013).
[61] L. Tzuang, K. Fang, P. Nussenzveig, S. Fan, and M. Lipson, Nat. Photon. **8**, 701 (2014).
[62] P. Roushan, C. Neill, A. Megrant, Y. Chen, R. Babbush, R. Barends, B. Campbell, Z. Chen, B. Chiaro, A. Dunsworth *et al.*, Nat. Phys. **13**, 146 (2017).
[63] I. Bloch, J. Dalibard, and S. Nascimbene, Nat. Phys. **8**, 267 (2012).
[64] A. L. C. Hayward, A. M. Martin, and A. D. Greentree, Phys. Rev. Lett. **108**, 223602 (2012).
[65] A. L. C. Hayward and A. M. Martin, Phys. Rev. A **93**, 023828 (2016).
[66] Y.-Y. Zhang, Z.-X. Hu, L. Fu, H.-G. Luo, H. Pu, and X.-F. Zhang, Phys. Rev. Lett. **127**, 063602 (2021).
[67] G. Calajó, F. Ciccarello, D. Chang, and P. Rabl, Phys. Rev. A **93**, 033833 (2016).
[68] H. Breuer and F. Petruccione, *The Theory of Open Quantum Systems* (Oxford University Press, Oxford, 2002).
[69] S. A. Hill and W. K. Wootters, Phys. Rev. Lett. **78**, 5022 (1997).
[70] J. Koch, T. M. Yu, J. Gambetta, A. A. Houck, D. I. Schuster, J. Majer, A. Blais, M. H. Devoret, S. M. Girvin, and R. J. Schoelkopf, Phys. Rev. A **76**, 042319 (2007).
[71] J. Majer, J. M. Chow, J. M. Gambetta, J. Koch, B. R. Johnson, J. A. Schreier, L. Frunzio, D. I. Schuster, A. A. Houck, A. Wallraff, A. Blais, M. H. Devoret, S. M. Girvin, and R. J. Schoelkopf, Nature (London) **449**, 443 (2007).
[72] P. Roushan, C. Neill, J. Tangpanitanon, V. M. Bastidas, A. Megrant, R. Barends, Y. Chen, Z. Chen, B. Chiaro, A. Dunsworth, A. Fowler, B. Foxen, M. Giustina, E. Jeffrey, J. Kelly, E. Lucero, J. Mutus, M. Neeley, C. Quintana, D. Sank *et al.*, Science **358**, 1175 (2017).
[73] M. Scigliuzzo, G. Calajó, F. Ciccarello, D. Perez Lozano, A. Bengtsson, P. Scarlino, A. Wallraff, D. Chang, P. Delsing, and S. Gasparinetti, Phys. Rev. X **12**, 031036 (2022).
[74] X. Zhang, E. Kim, D. K. Mark, S. Choi, and O. Painter, Science **379**, 278 (2023).
[75] B. R. Johnson, M. D. Reed, A. A. Houck, D. I. Schuster, L. S. Bishop, E. Ginossar, J. M. Gambetta, L. DiCarlo, L. Frunzio, S. M. Girvin, and R. J. Schoelkopf, Nat. Phys. **6**, 663 (2010).
[76] Z. H. Peng, J. H. Ding, Y. Zhou, L. L. Ying, Z. Wang, L. Zhou, L. M. Kuang, Y.-X. Liu, O. V. Astafiev, and J. S. Tsai, Phys. Rev. A **97**, 063809 (2018).
[77] R. Ma, B. Saxberg, C. Owens, N. Leung, Y. Lu, J. Simon, and D. I. Schuster, Nature (London) **566**, 51 (2019).